ADVANCED MATERIALS

Acceleration of Calcite Kinetics by Abalone Nacre Proteins**

By *Germaine Fu*, *S. Roger Qiu*,* *Christine A. Orme*, *Daniel E. Morse*, and *James J. De Yoreo*

The fascinating shapes and hierarchical designs of biomineralized structures have long been an inspiration to materials scientists because of the potential they suggest for biomolecular control over synthesis of crystalline materials.[1,2] One prevailing view is that mineral-associated macromolecules are responsible for initiating and stabilizing non-equilibrium crystal polymorphs and morphologies through interactions between anionic moieties and cations in solution or at mineral surfaces.[3–6] Indeed, numerous studies have demonstrated that bio-organic additives can dramatically alter crystal shapes and growth rates in vitro. However, previous molecular-scale studies revealing mechanisms of growth modification focused on small molecules such as amino acids or peptides and always observed growth inhibition. In contrast, previous studies using full proteins were non-quantitative, and underlying sources of growth modification were ill-defined.[7,8] Here we investigate interactions between proteins isolated from abalone shell nacre and growing surfaces of calcite. Surprisingly, we find that these proteins significantly *accelerate* the molecular-scale kinetics and, though much larger than atomic steps, alter growth morphology through step-specific interactions that appear to lower their free energies. Thus we propose that these proteins act as surfactants to promote ion attachment at calcite steps. Understanding the structural principles governing the control of these shape-modifying growth-accelerants could enable their exploitation in the production of crystalline materials.

Previous molecular studies have demonstrated that inorganic ions,[9–11] amino acids[5,6] and poly(aspartic acid) peptides[12] predominately interact with the step edges of growing hillocks on the existing crystals faces of calcite. Molecular modeling has shown that the strength of these interactions is much greater at steps than on terraces and is highly step-specific. Conversely, phenomenological studies of mineralization with full proteins—including ice inhibition—have assumed a stereochemical match of protein to crystal plane. Using results from in-situ atomic force microscopy (AFM) and scanning electron microscopy (SEM), here we show that two acidic proteins dramatically accelerate calcite growth while still altering the surface morphology through interactions with specific atomic steps on the (104) face. These two protein variants were isolated and purified from abalone shell nacre and designated AP8-α and AP8-β (*a*ragonite *p*roteins of 8 kDa, 1 Da = 1.66×10^{-27} kg). Parallel studies have shown that the AP8 proteins are potent growth modifiers.[13] Although in the true in-vivo situation these proteins are associated with aragonitic $CaCO_3$, we use the growth of calcite simply as an assay for the impact of acidic proteins on carbonate precipitation and to determine the mechanism and nature of changes in growth. Growth on pyramidal hillocks generated at dislocations was observed on a freshly cleaved (104) face of a calcite seed crystal exposed to supersaturated calcium carbonate solutions with a supersaturation ratio $S = 3$ (see Experimental section for definition of S). Growth hillocks exhibited the well-known rhombohedral shape of calcite, which is characterized by two pairs of structurally distinct, 3.1 Å-high steps related to one another by a c-glide plane as shown previously.[5] (These steps are commonly labeled obtuse and acute or positive and negative, with the former labels reflecting the angle formed between the step riser and the (104) plane.) Under the conditions of temperature, pH, ionic strength, and Ca to carbonate ratio used here (see Experimental), we found that, at $S = 3$, the obtuse steps grew faster than the acute, with the obtuse step speed $v_+ = 8.4$ nm s^{-1} and the acute step speed $v_- = 6.3$ nm s^{-1}. This difference causes the angle θ that bisects the two equivalent flanks of the growth hillock to deviate from 180° (Fig. 1a).

The AP8-β variant strongly alters both hillock morphology and step kinetics but selectively interacts to varying degrees with the two types of step edges. Figures 1a–f show the temporal progression of the growth hillock after 0.2 μM AP8-β protein was introduced to the solution. After approximately 1 h of continuous exposure to AP8-β protein, both acute step edges of the hillock became progressively less straight, eventually producing a rounded morphology (Figs. 1c–f). In contrast, the morphology of the obtuse step edges remained unchanged. These morphological changes, however, did not reach a steady state until 1 h after exposure to the protein-bearing solution.

In addition to altering step morphology, addition of AP8-β dramatically accelerated the step speeds, leading, for example, to an increase in the obtuse step speed by a factor of 4.8. At the same time, the acute step speed increased only by a factor of 2.1. As a result, the relative value of the obtuse to acute step speeds—and therefore the relative terrace widths—in-

[*] Dr. S. R. Qiu, Dr. C. A. Orme, Dr. J. J. De Yoreo
Department of Chemistry and Materials Science
Lawrence Livermore National Laboratory
P.O. Box 808, Livermore, CA 94551 (USA)
E-mail: qiu2@llnl.gov
G. Fu, Prof. D. E. Morse
Biomolecular Science and Engineering Graduate Program and
the Institute for Collaborative Biotechnologies
University of California at Santa Barbara
Santa Barbara, CA 93106 (USA)

[**] Support for this work was provided in part by the following agencies: the Department of Energy's Office of Basic Energy Sciences, Division of Chemical Sciences, Geosciences and Biosciences, and Division of Materials Science, the NASA University Research, Engineering and Technology Institute on Bio-Inspired Materials under No. NCC-1-02037, the University of California Biotechnology Research and Education Training Program, and the National Institutes of Health through grant DK61673. This work was performed under the auspices of the U.S. Department of Energy by the University of California, Lawrence Livermore National Laboratory under contract No. W-7405-Eng-48.

  DOI: 10.1002/adma.200500633

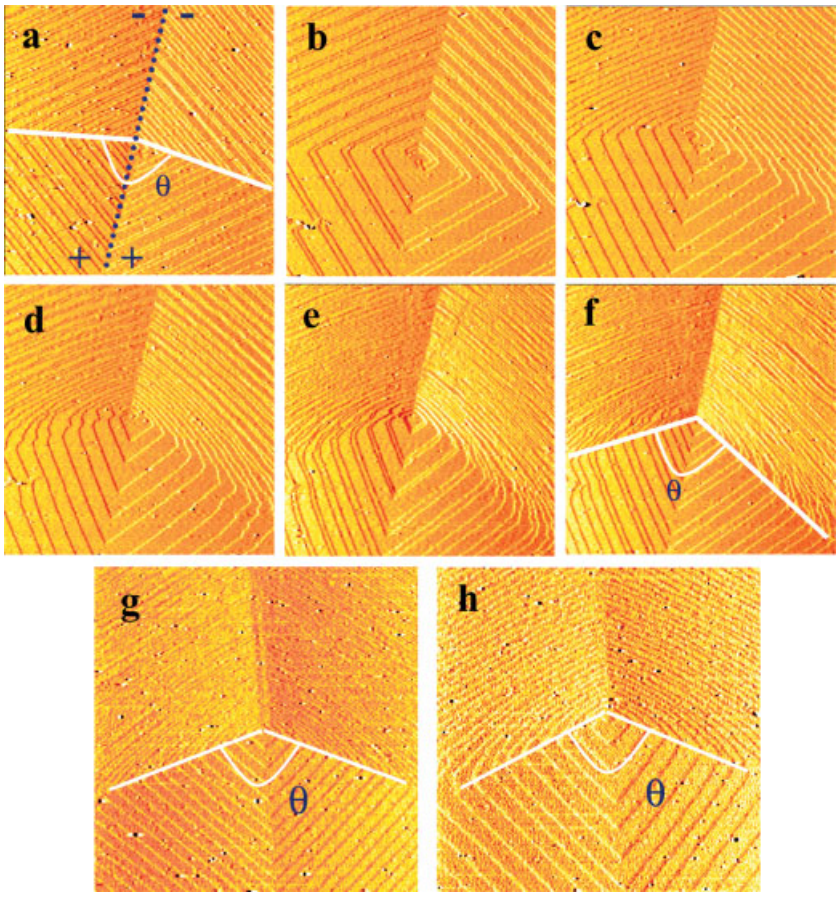

Figure 1. a) The growth under pure solution with $S=3$ ($t=0$ min). The paired flanks along the positive directions move faster than those along the negative directions. The difference in step speed along these two directions gives rise to $\theta<180°$. The dotted line shows the *c*-glide plane. b–f) Temporal progression of morphological changes induced by AP8-β protein. b) $t=50$ min, c) $t=70$ min, d) $t=90$ min, e) $t=110$ min, f) $t=122$ min. g,h) AFM images showing the steady-state morphology of dislocation hillocks after the effect of proteins AP8-β (g) and AP8-α (h) was fully realized. (Note that the trench in (g) at the corner of the acute steps was due to the interaction between multiple dislocation sources and does not reflect the action of the protein.) Horizontal scale: a–f) 3.4 μm; g,h) 5 μm.

creased by a factor of two. This also caused the reduction in angle θ, as seen in Figure 1f. However, the average terrace width for all steps, which scales with the step-edge free energy in a positive-definite manner,[14,15] decreased approximately by a factor of two.

The AP8-α protein was also a potent modifier of calcite growth, having a stronger effect than AP8-β on both morphology and kinetics. The changes induced by AP8-α also occurred at a much faster rate than those caused by AP8-β, with significant changes observed after only 10 min. To compare the extent of modulation by these two variants, we investigated the growth modification by both proteins under identical solution conditions including protein concentration (0.15 μM), induction time, solution pH, and temperature. Figures 1g,h show the morphologies of growth hillocks as modified by these two proteins after 1 h. In both cases, the acute step edges became rounded while the obtuse step edges remained straight, but the effect was slightly greater with AP8-α. Moreover, at this protein concentration, with AP8-α, the obtuse and acute steps advanced 3.3 and 2.3 times faster respectively, while with AP8-β, the increases were only 2.2 and 1.5 times faster, respectively.

The observed changes in step kinetics, step spacing, and hillock morphology provide important clues as to the mechanism by which AP8 proteins modify calcite growth. Despite the change in step speed and rounding of the hillocks at the length scale of this investigation, the step edges themselves remained smooth and showed no evidence of pinning sites in the presence of either protein variant. This is quite different from earlier observations, which showed that the entire mixture of soluble nacre proteins did generate pinning sites along the step edges.[16] The increase in step speed inferred from that study may well have been due to the presence of the AP8 variants in the protein mixture while other components of the mixture may have been responsible for the pinning at the step edge. The AP8 proteins alone clearly do not act as inhibitors that pin step motion.

The observed step acceleration is unlikely to be due to a change in calcite solubility as a result of AP8 incorporation, as was seen, for example, with addition of Mg^{2+} to calcite solutions,[13] because the AP8 concentration is far too small to produce a significant effect. Moreover, because acidic proteins tend to reduce Ca^{2+} activity in solution and would likely introduce strain into the crystal lattice, we would expect the incorporation of AP8 to lower the step speeds. Likewise, if AP8 acted to poison kink sites, the step speeds would decrease rather than increase. In fact, of the four end-member models for modification by additives[14,15]—1) step pinning, 2) incorporation, 3) kink poisoning, and 4) surfaction—an increase in step speed accompanied by changes in average step spacing and hillock shape without step pinning is consistent with only the fourth model. Thus, we postulate that, as with simple amino acids like aspartic acid,[6] AP8 proteins act as surfactants to modify the thermodynamics and kinetics of calcium and carbonate attachment at step edges without significant pinning, poisoning, or incorporation.

The structure of AP8 proteins should provide an understanding of these effects. The AP8 proteins are small proteins high in aspartic acid and glycine residues.[13] Numerical deconvolution of circular dichroism (CD) spectra[17] collected from AP8-α in Milli-Q (MQ) water (Fig. 2a) or in undersaturated

ADVANCED MATERIALS

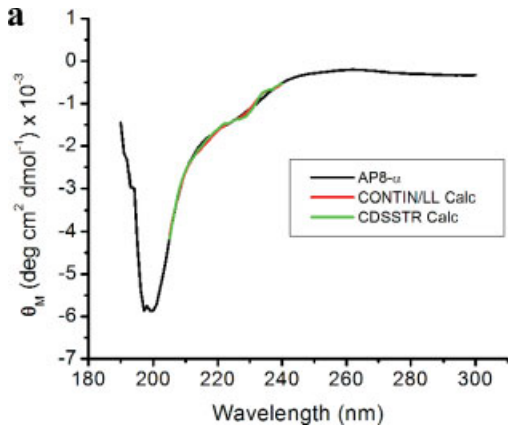

Method	% α	% β_s	% β_t	% U	% NRMSD
CONTIN/LL	5.4	38.4	22.5	33.7	3.0
CDSSTR	2.6	35.7	24.5	35.5	13.7
Average	4.0	37.1	23.5	34.6	

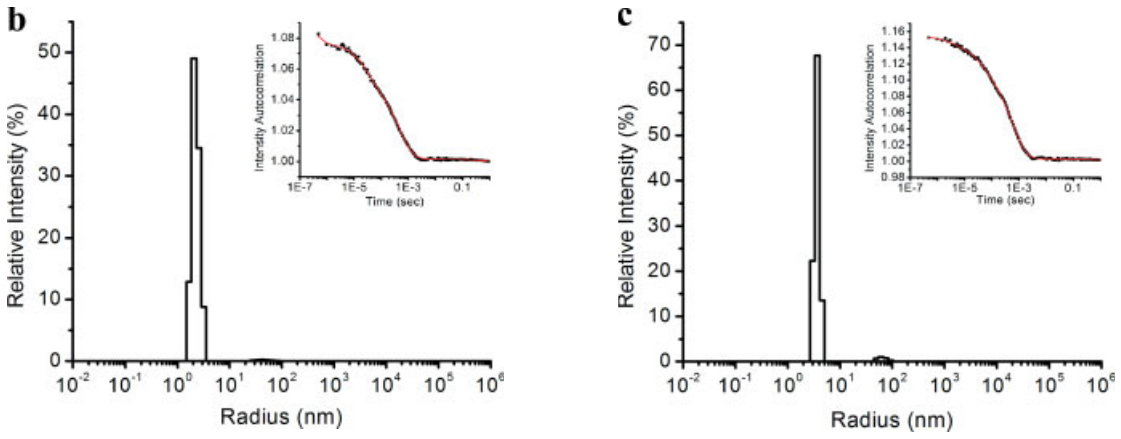

Figure 2. Solution structure of AP8-α. a) CD spectroscopy of AP8-α in MQ water and estimation of secondary structure fractions. The calculated CD spectra generated by the two methods of numerical deconvolution analyses are shown. α = alpha helix, βs = beta sheet, βt = beta turn, U = unordered, NRMSD = normalized root mean square deviation. b,c) Normalized hydrodynamic radius derived from dynamic light scattering analyses of AP8-α in MQ water (b) and 4 mM NH_4HCO_3 and 200 μM $CaCl_2$ (c). Insets show the normalized autocorrelation fluctuations of the scattered light intensity over logarithmic time. Points show acquired light scattering measurements and red lines represent fit to correlation functions after regularization analyses. (The CD spectrum for AP8-α in calcium carbonate buffer is not shown because it shows insignificant differences from that in MQ water.)

buffer containing calcium and bicarbonate ions (data not shown) revealed that the protein is approximately composed of the following secondary structure elements: 4.0 % α-helix, 37.1 % β-sheet, 23.5 % β-turn, and 34.6 % unordered structure (Fig. 2a). The contribution of discrete secondary structural elements to the CD spectrum is distinct from the random-coil spectra observed for the *N*-terminal peptides derived from two other abalone nacre proteins, AP7 and AP24.[18] Moreover, the predominance of beta structures in AP8-α argues for contiguous sequences of aspartic acid residues,[19,20] while additional domains of unordered structure may be attributed to the numerous glycine residues. These structural data suggest that the AP8 proteins may be amphiphiles.[21] In this case, the AP8 proteins may minimize interactions between ions or ion clusters in solution via an aggregation process in which the hydrophilic Asp domains are exposed and interacting with ions or water molecules, while the non-polar glycine residues remain shielded. The proposed protein–ion interaction in solution is supported by the observation that AP8-α solution structure changes in the presence of ions. In its native form, AP8-α has a hydrodynamic radius determined by dynamic light scattering of 2.3 nm (Fig. 2b). This experimentally determined dimension is larger than the theoretical hydrodynamic radius of 1.8 nm for a protein composed of 107 residues, suggesting that AP8-α may have an open rather than folded conformation. When calcium and bicarbonate ions were included in the buffer, the hydrodynamic radius of AP8-α shifted to 3.7 nm (Fig. 2c), which is slightly larger than the theoretical radius of 3.1 nm for completely denatured AP8-α. This increase in AP8-α radius was not observed when either calcium or bicarbonate ions were added individually to the solution (data not shown), indicating a change in structure was induced by multiple ion interactions or by interactions with small $CaCO_3$ nuclei. An increase in hydrodynamic radius may result from any of several events, or a combination thereof, including unfolding of the protein, binding of calcium ions, increased binding of the protein to solvent molecules, or an increase in protein aggregation. By possibly interfering with

the ability of the ions to interact with each other in solution, the AP8 proteins may increase the ion attachment rate to the steps on existing crystal faces. Alternatively, the proteins may transiently adsorb to the crystal surface and increase local supersaturation by carrying or attracting ions to the step edges. The AP8 proteins must then desorb from the surface before the ions can incorporate into the crystal lattice. This surfactant activity between the proteins and mineral-forming ions is distinct from the surface complementarity proposed for other crystal-controlling proteins, in which amino acid residues are rigidly presented by folded proteins, as in the case of osteocalcin binding to hydroxyapatite[22] and fish type I antifreeze proteins binding to ice.[23] Surprisingly, the AP8 proteins, which were selectively isolated as the most acidic from abalone shell nacre,[13] did not inhibit crystal nucleation and growth from solution, an activity generally postulated for acidic shell proteins.[24] Therefore, our observation of accelerated inorganic crystal growth induced by the addition of proteins may reflect a novel mechanism of surfaction between the AP8 proteins and mineral ions that promote ion attachment to the crystal surface.

Using SEM to image the crystal habit, we found that the changes observed at the elementary steps scale correlate well with changes seen in the macroscopic habit of calcite crystals grown in the presence of AP8 proteins. Calcium carbonate crystals grown de novo from solution by the slow diffusion method[13] typically form calcite rhombohedra of 10 to 50 μm in size (Fig. 3a). When crystals were grown in the presence of 1.2 μM of either AP8-α or -β protein, the morphology of calcite was strongly altered. The primary modification was the rounding of the two neighboring crystal edges formed by the acute steps of each (104) face. The crystal edges formed by the obtuse steps remained straight (Fig. 3b). Secondly, the bulk crystal size expanded in all directions but elongated predominantly along the *c*-axis as shown in Figure 3c. These images also show that there are roughened surfaces approximately parallel to the (001) planes that appear as macrosteps bridging the relatively smooth (104) faces. Such features are similar to those observed for aspartic acid[6,25,26] and Mg^{2+}.[9,11,27] Based on the hillock geometries seen in Figure 1, if one projects these shapes into three dimensions, the predicted progression of the crystal habit in the presence of AP8 proteins is as displayed in Figures 3d–f, which is identical to what is observed by SEM and similar to that predicted[11] and seen for Mg^{2+}.[27] The fact that the macroscopic crystal shape mimics the morphology of elementary steps at dislocation hillocks indicates that the interaction between the proteins at the step edges is directly responsible for the modification of the macroscopic crystal habit.

Strict morphological control over crystal size, shape, and texture is one of the remarkable aspects of biogenic minerals. However, the multitude of studies describing altered morphologies for crystals grown in vitro in the presence of additives including proteins have never produced the elaborate morphologies found in nature. The reason for this is likely to reflect the fact that the simplified systems used to recapitulate in-vivo crystal growth are based on an incomplete description of the microenvironment in which mineralization occurs in organisms. Our study is no exception. However, the specific and novel effect of the AP8 proteins on calcite hillock morphology and step kinetics demonstrates a unique molecular description of protein–crystal interaction. Considering the scarcity of data that exists on the function of individual proteins from biogenic $CaCO_3$, our hope is that elucidation of the mechanistic basis of the AP8-calcite interaction may ultimately provide insight into the proteins' role in stabilizing aragonite biosynthesis during formation of the shell. Therefore, although the biological significance of our results remains to be determined, the novel phenomenon of surfactant activity that increases step speed contributes to our fundamental understanding of crystal-growth control by acidic proteins and polymers and may be exploited for future materials development.

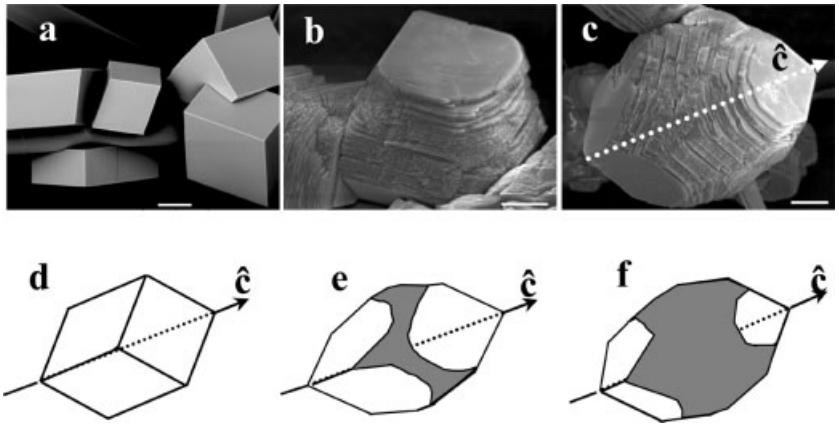

Figure 3. SEM images of macroscopic calcite crystals grown de novo from solution by slow diffusion. a) Smooth calcite rhombohedra grown in the absence of additives. b,c) Calcite crystals grown in the presence of 10 μg mL^{-1} AP8-α for three days. In (b), each rhombohedral face of the crystals exhibits rounded acute edges, while the obtuse edges remain unmodified and straight. In (c), a modified calcite crystal was imaged at a different viewing angle to show that the crystal habit was elongated along the c-axis and capped by rhombohedral faces. Scale bar dimensions: a) 10 μm, b,c) 5 μm. d–f) Geometric model showing the evolution of the bulk crystal habit under the influence of AP8 proteins. The {104} planes are in white and the newly expressed surfaces are shaded in grey.

In conclusion, we have shown that the AP8 proteins significantly accelerate the kinetics and modify the shape of growing calcite through step-specific interactions, although the size of these proteins is significantly larger than that of the atomic steps. The decrease in average terrace width suggests that these protein variants reduce the step-edge free energy. Moreover, structural analyses of the AP8 proteins further support the hypothesis that these proteins act as surfactants to increase the rate of ion attachment at the calcite step edge.

ADVANCED MATERIALS

Experimental

In-Situ Atomic Force Microscopy and Solution Preparation: Micrographs on the (104) face of calcite crystal (Iceland spar variety, Ward's Natural Science, Rochester, NY) were collected in contact mode with a Nanoscope III instrument (Digital Instruments, Santa Barbara, CA) during the growth events. A typical seed crystal was about 1 cm^3 in size and was glued with polyurethane onto a glass cover slip that was attached to the metallic AFM specimen discs (Ted Pella). Before each experiment, the crystal was cleaved so a fresh (104) surface was exposed. The O-ring in the liquid cell was directly placed on top of the (104) face, and a tight seal was formed between the cell and the seed crystal. Typically, the seed crystal was oriented in such a way that the *c*-glide plane of the (104) face was perpendicular to the AFM fast-scan axis (Fig. 1). All experiments were performed at 24 °C.

The supersaturated calcium carbonate solution ($S = 3$) was made by mixing 23 mM $NaHCO_3$ with 0.24 mM $CaCl_2$ at equal volumes. The supersaturation ratio was determined by $S = a(Ca^{2+})\,a(CO_3^{2-})/K_{sp}$ using Geochemist's Workbench, where $a(Ca^{2+})$ and $a(CO_3^{2-})$ are the activities of the calcium and carbonate ions respectively, and K_{sp} (where $K_{sp} = 3.3 \times 10^{-9}$) is the calcite solubility product. Before adding in proteins, the pure solution was filtered through a 0.22 μm filter (Millipore). The final pH of the pure or protein-doped solutions remained unadjusted at 8.8.

In each experiment, the images were obtained while supersaturated solutions were flowing through the system. The flow rate (2 mL min^{-1}) was adjusted to ensure that growth was limited by surface kinetics and not by diffusion. To eliminate the imaging artifacts and perturbation to growth kinetics, the imaging force was reduced to the minimum possible value that allowed the tip to remain in contact with the surface. Since the in-situ images were taken in real time, it is inevitable that distortion of the step orientation will exist in the images. Such distortion is caused by the step movement during the finite scan time so that its apparent direction differs from the true orientation. The images reported here were not corrected for this effect. In fact, we used this change in angle to extract the step velocities at different growth conditions [28].

Protein Isolation and Purification: The AP8 proteins were isolated from abalone shell nacre and the variants were purified by high-pressure liquid chromatography as previously described [13]. Isolation of the individual AP8-α and -β proteins from each other was confirmed by the presence of single bands in sodium dodecylsulfate–poly(acrylamide) gel electrophoresis (SDS-PAGE) gels and by single peaks in matrix-assisted laser desorption ionization time-of-flight (MALDI-TOF) mass spectra that corresponded to only one of the two variants. The AP8 proteins were also distinguished by their unique amino acid compositions. Protein fractions were resuspended in MQ water for quantification by amino acid analysis, and aliquots were stored at –80 °C until use.

Circular Dichroism Spectroscopy: CD spectra of the AP8-α protein were collected using a Circular Dichroism Spectrometer, Model 202, from AVIV Instruments, Inc (Lakewood, NJ), running Aviv CDS software, version 2.96. The protein sample was resuspended in MQ water at a concentration of 38.4 μM and scanned from 190 to 300 nm at 22 °C, sampling every 1 nm for 60 s. The experimental spectrum was the average acquired over 8 scans. Mean residue ellipticity [θ_M] is expressed in deg cm^2 $dmol^{-1}$ per mole protein. Secondary structure estimations based on CD spectra from 205 to 240 nm were calculated using the CDPro software programs CONTIN/LL and CDSSTR for CD analysis using a set of 43 soluble proteins with known crystal structures as references for numerical deconvolution [17]. The degree of similarity between the average experimental and calculated (reconstructed) CD spectra is expressed as the normalized root mean square deviation (NRMSD) for each method [29]. NRMSD values below 15 % are considered acceptable and below 5 % are excellent [30]. Results from two methods are shown to demonstrate convergence towards similar fraction values.

Dynamic Light Scattering: Purified AP8-α protein was resuspended in MQ water or buffer (4 mM NH_4HCO_3, 200 μM $CaCl_2$, pH 8.3) that had been passed through a 0.22 μm filter to a final protein concentration of 25–30 μM. The protein solution was centrifuged at 20 800 rcf for 30 min and transferred to a dust-free 10 μL quartz light-scattering microcuvette. Dynamic light scattering measurements were collected at room temperature (22 °C) with a quasi-elastic light scattering (QELS) detector attached to a miniDAWN instrument from Wyatt Technology Corp. (Santa Barbara, CA) equipped with a laser diode ($\lambda_0 = 690$ nm) and a multiple tau, 264 channel autocorrelator. Scattered light was detected at 90° in batch mode and autocorrelation functions of the scattered light were recorded. Data acquisition and processing were performed by Astra V software with the QELSBatch configuration. For the polydisperse AP8-α samples, the autocorrelation functions of the scattered light intensity were described by the following pair of equations used in the DYNALS computational algorithm (Alango Ltd, Israel):

$$g^{(2)}(t) = [g^{(1)}(t)]^2 + 1 + \zeta(t) \quad (1)$$

$$g^{(1)}(t) = \int_0^\infty P(\Gamma)\exp(-\Gamma t)\mathrm{d}\Gamma \quad (2)$$

The decay rate Γ of the signal reflects the free movement of the particles and is directly proportional to the translational diffusion coefficient D ($D = \Gamma/q^2$, where q is the scattering vector). The mean hydrodynamic radius (r_h) for a population of particles in solution is inversely proportional to D, as described in the Stokes–Einstein equation for spherical particles: $r_h = kT/6\pi\eta D$, where kT is the Boltzmann temperature and η is the viscosity of the solution. To include the effects of polydispersity, regularization analysis of the decay time distribution with the DYNALS algorithm determines the function $P(\Gamma)$, which is the proportion of the sample with a given decay time Γ. Each decay rate Γ is related to a different size, and the mean hydrodynamic radius is an average of the distribution of sizes determined.

Calculations for the theoretical native and denatured hydrodynamic radii of AP8-α were based on the following equations [31]:

For native proteins,

$$\ln(r_h) = 0.29\ln(\text{number of residues}) + 1.56 \quad (3)$$

For denatured proteins,

$$\ln(r_h) = 0.57\ln(\text{number of residues}) + 0.79 \quad (4)$$

The equations describe the linear relationship between the ln(number of residues) and ln(hydrodynamic radius in Å) derived from a reference set of proteins under native and denaturing conditions. The total number of residues in AP8-α was based on average number of nanomoles detected for each amino acid over twelve analyses, and a MALDI-TOF mass of 8707.55 for the protein [13].

Scanning Electron Microscopy: Calcite crystals were grown by slow diffusion for SEM analysis as previously described [13]. Briefly, polyamide Kevlar fibers were used as the substrate for crystal growth from a solution of 12 mM $CaCl_2$. The submerged fibers were placed in wells of a tissue culture plate covered with foil punched with pinholes. The multi-well plates were sealed in a desiccator with a dish of solid ammonium carbonate, which slowly released CO_2 gas that upon acidification in aqueous solution formed bicarbonate ions. To grow protein-modified crystals, the purified AP8 variants were added to the $CaCl_2$ solution at a concentration of 10 μg mL^{-1} (equivalent to 1.2–1.3 μM). After 3 days of growth, the crystal-coated fibers were rinsed in methanol and allowed to completely dry at 37 °C for several hours before they were sputter-coated with gold in preparation for imaging with a Tescan VEGA TS 5130MM scanning electron microscope.

Received: March 26, 2005
Final version: June 28, 2005
Published online: October 11, 2005

[1] L. Addadi, S. Weiner, in *Biomineralization: Chemical and Biochemical Perspectives* (Eds: S. Mann, J. Webb, R. J. P. Williams), VCH, Weinheim, Germany **1989**, Ch. 5.
[2] S. Mann, *Biomineralization: Principles and Concepts in Bioinorganic Materials Chemistry*, Oxford University Press, Oxford, UK **2001**.
[3] M. Fritz, A. M. Belcher, M. Radmacher, D. A. Walters, P. K. Hansma, G. D. Stucky, D. E. Morse, S. Mann, *Nature* **1994**, *371*, 49.
[4] S. R. Qiu, A. Wierzbicki, C. A. Orme, A. M. Cody, J. R. Hoyer, G. H. Nancollas, S. Zepeda, J. J. De Yoreo, *Proc. Natl. Acad. Sci. USA* **2004**, *101*, 1793.
[5] H. H. Teng, P. M. Dove, J. J. De Yoreo, *Geochim. Cosmochim. Acta* **1999**, *63*, 2507.
[6] C. A. Orme, A. Noy, A. Wierzbicki, M. T. McBride, M. Grantham, H. H. Teng, P. M. Dove, J. J. De Yoreo, *Nature* **2001**, *411*, 775.
[7] S. Geider, A. Baronnet, C. Cerini, S. Nitsche, J. P. Astier, R. Michel, R. Boistelle, Y. Berland, J. C. Dagorn, J. M. Verdier, *J. Biol. Chem.* **1996**, *271*, 26 302.
[8] A. Berman, L. Addadi, S. Weiner, *Nature* **1988**, *331*, 546.
[9] K. J. Davis, P. M. Dove, J. J. De Yoreo, *Science* **2000**, *290*, 1134.
[10] L. E. Wasylenki, P. M. Dove, D. S. Wilson, J. J. De Yoreo, *Geochim. Cosmochim. Acta* **2005**, *69*, 3017.
[11] K. J. Davis, P. M. Dove, L. E. Wasylenki, J. J. De Yoreo, *Am. Mineral.* **2004**, *89*, 714.
[12] S. Elhadj, N. Han, P. M. Dove, E. Salter, A. Wierzbicki, J. J. De Yoreo, *EOS Trans. AGU* **2004**, *85*, B21B-0871.
[13] G. Fu, S. Valiyaveettil, B. Wopenka, D. E. Morse, *Biomacromolecules* **2005**, *6*, 1289.
[14] J. J. De Yoreo, P. G. Vekilov, in *Biomineralization*, Vol. 54 (Eds: P. M. Dove, J. J. De Yoreo, S. Weiner), The Mineralogical Society of America, Washington, DC **2003**, p. 57.
[15] P. M. Dove, J. J. De Yoreo, K. J. Davis, in *Nanoscale Structure and Assembly at Solid–Fluid Interfaces*, Vol. 2 (Eds: X. Y. Liu, J. J. De Yoreo), Kluwer Academic, New York **2004**, p. 55.
[16] D. A. Walters, B. L. Smith, A. M. Belcher, G. T. Paloczi, G. D. Stucky, D. E. Morse, P. K. Hansma, *Biophys. J.* **1997**, *72*, 1425.
[17] N. Sreerama, R. W. Woody, *Anal. Biochem.* **2000**, *287*, 252.
[18] M. Michenfelder, G. Fu, C. Lawrence, J. C. Weaver, B. A. Wustman, L. Taranto, J. S. Evans, D. E. Morse, *Biopolymers* **2003**, *70*, 522.
[19] J. S. Evans, S. I. Chan, W. A. Goddard, *Protein Sci.* **1995**, *4*, 2019.
[20] S. Weiner, L. Addadi, *Trends Biochem. Sci.* **1991**, *16*, 252.
[21] D. W. P. M. Luwik, J. C. M. van Hest, *Chem. Soc. Rev.* **2004**, *33*, 234.
[22] Q. Q. Hoang, F. Sicheri, A. J. Howard, D. S. C. Yang, *Nature* **2003**, *425*, 977.
[23] J. Baardsnes, L. H. Kondejewski, R. S. Hodges, H. Chao, C. Kay, P. L. Davies, *FEBS Lett.* **1999**, *463*, 87.
[24] B.-A. Gotliv, N. Kessler, J. L. Sumerel, D. E. Morse, N. Tuross, L. Addadi, S. Weiner, *ChemBioChem* **2005**, *6*, 304.
[25] S. Mann, J. M. Didymus, N. P. Sanderson, B. R. Heywood, *J. Chem. Soc., Faraday Trans.* **1990**, *86*, 1873.
[26] D. B. DeOliveira, R. A. Laursen, *J. Am. Chem. Soc.* **1997**, *119*, 10 627.
[27] Y.-J. Han, J. Aizenberg, *J. Am. Chem. Soc.* **2003**, *125*, 4032.
[28] T. A. Land, J. J. De Yoreo, J. D. Lee, *Surf. Sci.* **1997**, *384*, 136.
[29] S. Brahms, J. Brahms, *J. Mol. Biol.* **1980**, *138*, 149.
[30] B. R. Baker, R. L. Garrell, *Faraday Discuss.* **2004**, *126*, 209.
[31] D. K. Wilkins, S. B. Grimshaw, V. Receveur, C. M. Dobson, J. A. Jones, L. J. Smith, *Biochemistry* **1999**, *38*, 16 424.

Magnetic Nanocrescents as Controllable Surface-Enhanced Raman Scattering Nanoprobes for Biomolecular Imaging**

By *Gang L. Liu*, *Yu Lu*, *Jaeyoun Kim*, *Joseph C. Doll*, and *Luke P. Lee**

Surface-enhanced Raman scattering (SERS) spectroscopy shows chemical-bond information, and it is one of the best methods for label-free biomolecular imaging. Conventional SERS substrates require multiple plasmonic couplings via many colloidal nanoparticles, and it is difficult to control the coupling distance. Here, we report the design, fabrication, and characterization of a biocompatible composite (Au/Ag/Fe/Au) nanocrescent SERS nanoprobe, which can not only function as a standalone SERS substrate with integrated SERS hot-spot geometries, but can also be controlled magnetically to produce orientational and translational motions. A single nanocrescent demonstrates a SERS enhancement factor higher than 10^8 in the detection of sub-zeptomole molecular concentrations. Magnetically modulated SERS detection of molecules on a single composite nanocrescent probe is demonstrated. The gold surfaces of composite nanocrescent SERS probes are biocompatible, and thus they can be biofunctionalized and applied in real-time biomolecular imaging.

Unlike conventional fluorescence imaging, Raman spectroscopy acquires unique signatures of chemical and biological molecules without labeling with fluorophore molecules.[1] Raman imaging of living cells can nondestructively probe the intracellular biochemical dynamics without prior fluorescent or radioactive labeling,[2] but the formidably low efficiency of Raman scattering hinders its applications in the detection of molecules at micromolar or lower concentrations. However, SERS by metallic nanostructures increases the original Raman scattering intensity for many orders of magnitude, which makes the Raman detection of low concentration molecules practical.[3] Colloidal Au or Ag nanoparticle clusters are commonly used as SERS substrates, and Raman enhancement factors as high as 10^{14} have been reported in single-molecular-

[*] Prof. L. P. Lee, G. L. Liu, Dr. Y. Lu, Dr. J. Kim, J. C. Doll
Biomolecular Nanotechnology Center and
Berkeley Sensor and Actuator Center
Department of Bioengineering, University of California-Berkeley
Berkeley, CA 94720 (USA)
E-mail: lplee@berkeley.edu

[**] We appreciate Dr. Y. Yin and Prof. A. P. Alivisatos in the Molecular Foundry at the Lawrence Berkeley National Laboratory for assistance with TEM imaging. This work is supported by DARPA and Samsung Electronics. J. K. was supported by a grant (05K1501-02810) from the Center for Nanostructured Materials Technology under 21st Century Frontier R&D Programs of the Ministry of Science and Technology, Korea. Supporting Information is available online from Wiley InterScience or from the author.

 DOI: 10.1002/adma.200501064